How to cite: *Angew. Chem. Int. Ed.* **2023**, *62*, e202303585
doi.org/10.1002/anie.202303585

Photocatalysis

A General Organophotoredox Strategy to Difluoroalkyl Bicycloalkane (CF2-BCA) Hybrid Bioisosteres**

*Sara Cuadros, Giulio Goti, Giorgia Barison, Alfredo Raulli, Tommaso Bortolato, Giorgio Pelosi, Paolo Costa, and Luca Dell'Amico**

Dedicated to Professor Paolo Melchiorre on the occasion of his 50th birthday

Abstract: Here, we report a general approach to the synthesis of the difluoroalkyl bicycloalkanes (CF_2-BCAs), as structural surrogates of aryl ketones and ethers. The chemistry is driven by a dihydrobenzoacridine photocatalyst, that engages in a catalytic electron-donor acceptor (EDA) complex, or directly reduces the fluorinated substrate. These two convergent manifolds lead to the generation of the R-CF_2 radical, that reacts with the [1.1.1]- or [3.1.1.]-propellane. The method is extremely general, and extendable to complex bioactive molecules (30 examples, up to 87% yield). The structural features of the CF_2-BCP hybrid bioisostere were investigated by single crystal X-ray. Finally, we synthesised a CF_2-BCP analogue of a Leukotriene A_4 hydrolase inhibitor, replacing the original aryl ether motif. In silico docking studies indicated that this new analogue maintains the same arrangement within the enzyme pocket, profiling the use of the CF_2-BCA hybrid bioisostere in medicinal chemistry settings.

Introduction

The bioisosteric replacement is a fundamental tool in medicinal chemistry to tune the physicochemical and biological properties of a drug. This strategy is based on the substitution of a chemical motif with another functionality, without altering the key interactions for molecular recognition.[1] Of particular interest are the bioisosteres that can replace widely present chemical units in bioactive molecules. In this regard, the difluoromethylene group ($-CF_2-$) is a suitable replacement of carbonyl groups (C=O) or oxygen atoms, inferring to the parent molecule an enhanced potency and/or pharmacokinetic profile.[1c] For example, the introduction of a $-CF_2-$ group in **1** (Figure 1a) led to an increased inhibitory activity towards Leukotriene A_4 (LTA_4) hydrolase, while other functionalities showed inferior effects.[2] On the other hand, bicyclopentanes

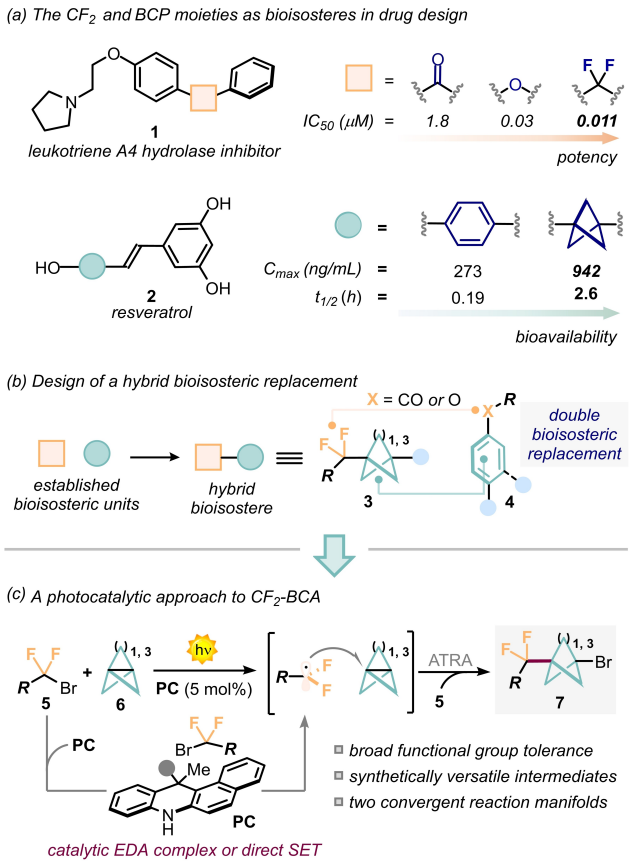

Figure 1. a) Examples of the use of CF_2 and BCPs as hybrid bioisosteres. b) This work: Design of new fluorinated fragments for bioisosteric replacement. c) Photo-organocatalytic strategy to the CF_2-BCA unit.

[*] Dr. S. Cuadros, Dr. G. Goti, G. Barison, A. Raulli, T. Bortolato, Dr. P. Costa, Prof. L. Dell'Amico
Department of Chemical Sciences, University of Padova
Via Francesco Marzolo 1, 35131 Padova (Italy)
E-mail: luca.dellamico@unipd.it
Prof. G. Pelosi
Department of Chemistry, Life Sciences and Environmental Sustainability, University of Parma
Parco Area delle Science 17, 43124 Parma (Italy)

[**] A previous version of this manuscript has been deposited on a preprint server (https://doi.org/10.26434/chemrxiv-2023-vdvlw).

(BCPs) and bicycloheptanes (BCHeps) have emerged as promising bioisosteres of *para*- and *meta*-substituted aromatic rings, respectively.[1d,3] Interestingly, these moieties can infer improved water solubility avoiding π–π interactions, and a higher resistance to oxidative metabolic processes, as exemplified with the BCP-resveratrol **2** (Figure 1a).[4] The merger of two structural bioisosteres into a new hybrid functionality has recently attracted the attention of the scientific community (Figure 1b). Pioneering contributions in this field have involved the design of multivicinal fluoroalkanes,[5a] and SF_5–BCPs.[5b] By merging two bioisosteres, it is possible to give rise to a number of new molecules with improved biological activity. This approach is in great demand, especially within drug discovery programs.[6] However, in spite of its potential applications in synthetic and medicinal chemistry settings, general methods to combine established bioisosteric units are largely underdeveloped.[5,7]

Herein, we document the design and implementation of a mild photocatalytic strategy to access CF_2–BCA (bicycloalkane) hybrid bioisosteres **7** (Figure 1c). Our light-driven approach builds on the activity of an organic photocatalyst (PC), that can generate the reactive R–CF_2 radical through two alternative yet convergent mechanisms. The PC can form a catalytic electron-donor-acceptor (EDA) complex with the aromatic substrates or directly reduce the other types of difluoroalkyl precursor **5**.[8] Light excitation of the EDA complex promotes a single-electron transfer (SET) that leads to the generation of a difluoromethylene radical, engaging in an atom-transfer radical addition (ATRA) with propellane **6**.

The method is general and extendable to highly diversified scaffolds, including complex bioactive ingredients.[9] The synthetic versatility of the CF_2–BCA **7** was proved with various manipulations. To evaluate the structural features of the hybrid bioisosteres in the solid state, we performed single crystal X-ray analysis on selected products. Finally, the CF_2–BCP hybrid bioisostere was installed into a known Leukotriene A_4 (LTA_4) hydrolase inhibitor, whose interactions with the enzyme were evaluated by means of docking studies.

Results and Discussion

Optimization Study and Mechanistic Investigations

Our investigation began by evaluating the performance of (bromodifluoromethyl) phenylsulfone **8** as a radical precursor, under the conditions described in Table 1. We selected this substrate since the sulfonyl moiety (–SO_2Ph) can be easily removed under reductive conditions, giving access to the valuable –CF_2H functionality.[10]

We initially tested the performance of different highly reducing PCs, including phenothiazine **PC1**, the naphthochromenone (**PC2**), 12-aryl dihydrobenzoacridine (12ADBA, **PC3**)[11] and the trisubstituted phenolate **PC4**, developed by our group (Table 1, entries 1–4).[12] Satisfactorily, we found the best performance with **PC3**, obtaining the desired CF_2–BCP product **10** in 89% NMR yield after

Table 1: Optimization of the reaction conditions and control experiments—selected results.[a] Reactions performed at 0.2 mmol scale, using 1 equiv of **8** and 1 equiv of **9** (see Supporting Information).[b] The yields were determined by ^{1}H NMR analysis, using trichloroethylene as internal standard. Isolated yields are reported in parenthesis.[c] Reaction time: 2 h.

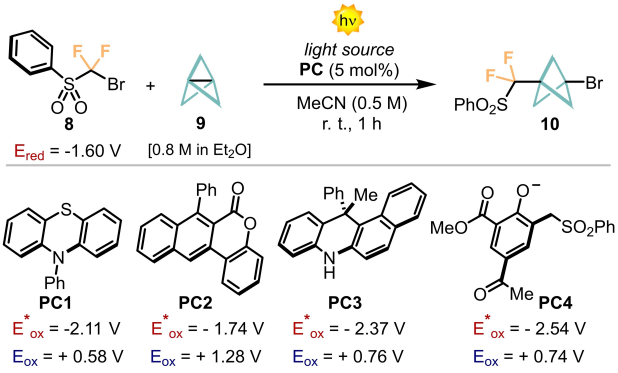

Entry[a]	photocatalyst	light	10 yield (%)[b]
1	PC1	Kessil, 400 nm (45 W)	61
2	PC2	Kessil, 400 nm (45 W)	87
3	PC3	Kessil, 427 nm (45 W)	89
4	PC4	Kessil, 456 nm (45 W)	80
5[c]	PC3	**Kessil, 427 nm (45 W)**	**96 (70)**
6	PC3	*light off*	*traces*
7	none	Kessil, 427 nm (45 W)	0

1 h (entry 3). Increasing the reaction time to 2 h allowed the full conversion of the starting material **8**, forming the product **10** in 96% NMR yield (70% isolated yield, entry 5). No product was detected in the absence of light (entry 6) or without PC (entry 7), revealing the photocatalytic nature of the process.

Our next efforts were directed towards the elucidation of the mechanism of this light-triggered radical process. The analysis of the optical absorption spectra of the reaction components showed a clear red-shift when **PC3** was mixed with an increasing amount of the sulfone **8**. This behavior suggests the possible formation of an EDA complex (Figure 2a). By UV/Vis Job plot analysis, we determined the molar ratio of the species involved in the complex to be 1:1 (see Supporting Information, section G.6). To gain further insights into the nature of this complex, we performed a series of spectroscopic and computational analyses. ^{1}H NMR titration experiments ruled out the hypothesis of having H-bonding interactions between **PC3** and **8** (See Supporting Information, section G.5). These results are in agreement with the DFT calculations (M06-2x/Def2TZVP/IEFPCM-(CH3CN)), since amongst the different complexes computed, including H-bonding and halogen-bonding ones, the most stable are characterized by a π–π interaction between the aromatic core of **PC3** and the phenyl ring of the sulfone (see Supporting Information, section H).

Interestingly, the HOMO lies entirely on the **PC3**'s core while the LUMO is located on the sulfone **8**, and it is

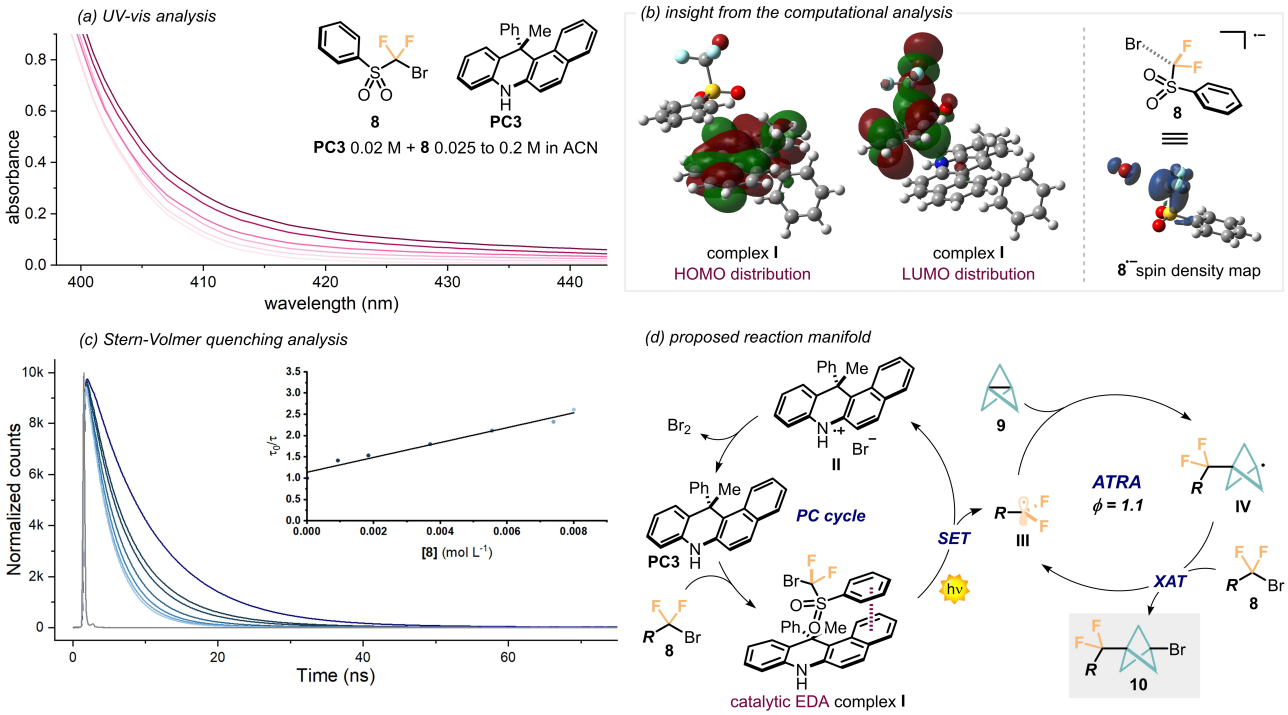

Figure 2. a) Ultraviolet absorption spectra of **PC3** with increasing amount of **8**. The colour intensity corresponds to increasing amount of **8**, i.e. 0.025 mmol per addition. b) Computational analysis of selected reaction intermediates. c) Lifetime decay of **PC3** and Stern–Volmer quenching of **PC3** with **8**. In the inset on the right is shown the plot of τ_0/τ as a function of the quencher concentration [**8**]. d) Proposed mechanism for the organophotoredox catalyzed difluoroalkylation of propellanes.

distributed all along the molecule structure (Figure 2b). Moreover, TD-DFT calculations at the same level of theory predict a red-shift of the computed UV/Vis spectrum of the π–π complex which agrees with the experimental observation. To provide information on the initiation step, we carried out Stern–Volmer quenching studies. Here, increasing amounts of the bromide **8** could effectively quench the excited state fluorescence of **PC3**, whereas no quenching was observed with the propellane solution **9** (Supporting Information, section G.4). To investigate the possibility of alternative productive pathways, we evaluated the contribution of a dynamic quenching through time-resolved fluorescence decay of **PC3** excited state (Figure 2c). Indeed, we observed a linear correlation between the **PC3** lifetime (τ_0/τ) and concentration of **8**, indicating that a SET under diffusional control can occur ($k_q = 1.95 \times 10^{10}\ M^{-1} s^{-1}$). Based on these results, we propose two alternative initiation steps, both converging into an ATRA manifold (Figure 2d). The direct excitation of **PC3** or the excitation of the EDA complex **I**, lead to the reactive intermediate **III**, with the concomitant formation of the **PC3**'s radical cation **II**. DFT analysis of **8**$^{\bullet-}$ shows that the C–Br bond is almost entirely dissociated, with a bond length between the CF_2 carbon and the bromine atom of 2.99 Å. Interestingly, the spin density map (Figure 2b, right) revealed that the unpaired electron is mostly located at the CF_2 carbon, thus corroborating the indirect experimental evidence for the formation of the reactive radical intermediate **III**.

Having determined a reaction quantum yield (QY) value of 1.1, and in agreement with other literature reports,[13] we confirmed an ATRA manifold, where **III** adds to **9** through a strain-release process, affording the open-shell intermediate **IV**. This radical species undergoes halogen-atom transfer (XAT) with another molecule of **8**, giving the product **10**, while regenerating the reactive difluoroalkyl radical **III**. At the other side of the photoredox cycle, the **PC3**'s ground state is regenerated by reduction of the Br anion ($E_{ox} = +0.71$ V vs SCE).[14]

Generality of the Process

After having elucidated the reaction manifold, we evaluated the generality of the developed photocatalytic process. As shown in Table 2, a wide array of difluoroalkyl bromides **5** proved to be suitable for this transformation. It is worth noting that previous photocatalyzed ATRA processes with difluoroalkyl bromides have typically suffered from inefficient initiation and/or atom transfer steps, thus limiting the scope of radical precursors to biased substrates.[15] Sulfur derivatives, including substituted aryl sulfones (**10**–**13**), thioethers (**14**–**18**), as well as aryl sulfoxide (**19**), were successfully used under the ATRA process, leading to the corresponding CF_2–BCP products in good to high yields (up to 79 %). Both [1.1.1]- and [3.1.1]-propellanes reacted equally well (70 % yield for **10** vs 84 % yield for **11**). Noteworthy, amine derivatives proved to be useful starting

Table 2: Scope of the reaction for the precursors **5** and **6**. Reactions performed on 0.2 mmol scale with 1 equiv of **5** and **6**. Isolated yields are reported.[a] 1.5 equiv of CF_2Br_2 was used (see Supporting Information for details).

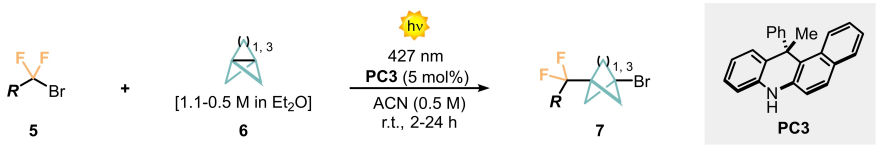

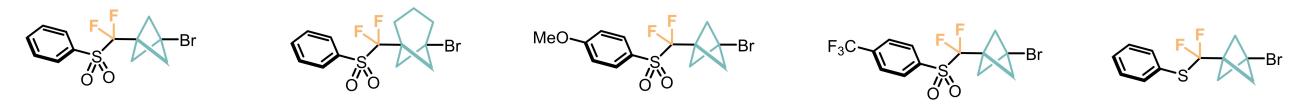
10, 70% yield
1 mmol scale, 221 mg

11, 84% yield

12, 49% yield

13, 51% yield

14, 54% yield

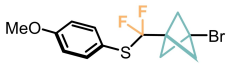
15, 55% yield

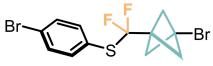
16, 46% yield

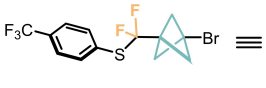
17, 64% yield

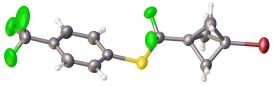
CCDC 2226178


18, 67% yield

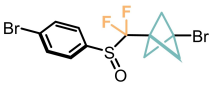
19, 27% yield

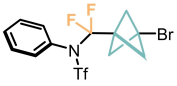
20, 71% yield

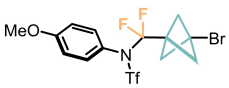
21, 81% yield

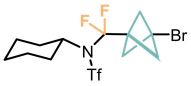
22, 86% yield

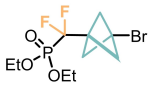
23, 47% yield

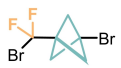
24, 85% yield[a]


25, 55% yield[a]

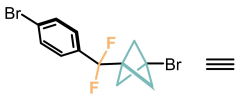
26, 64% yield

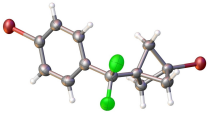
CCDC 2217587

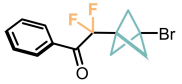
27, 69% yield

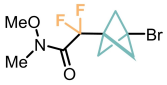
28, 70% yield

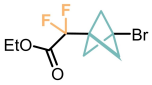
29, 70% yield


30, 42 %yield

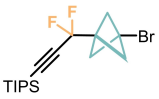
31, 87% yield

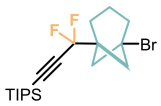
32, 84 %yield

biologically relevant substrates

from paracetamol

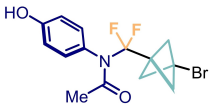
33, 33% yield

from tyramine

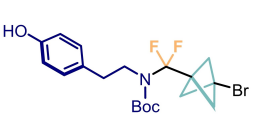
34, 39% yield

from D-galactose

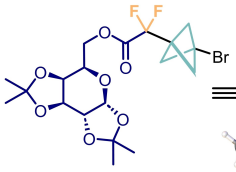
35, 76% yield

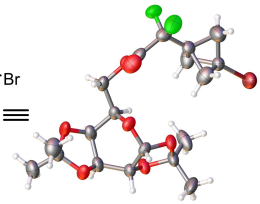
CCDC 2226179

from NH_2-Gly-Ala-OMe

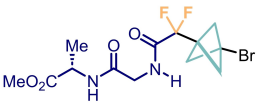
36, 75% yield

from tryptophan

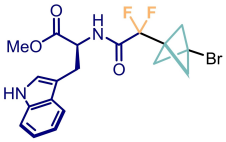
37, 68% yield

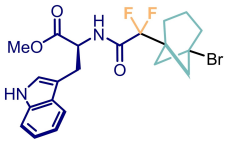
38, 75% yield

from L-phenylalanine

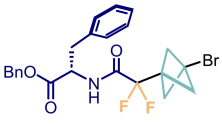
39, 56% yield

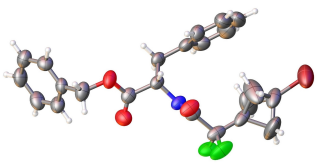
CCDC 2217588

materials, delivering the corresponding products **20**–**22** in high yields (up to 87 %). To the best of our knowledge, this is the first example on the use of bromo(difluoromethyl)amines derivatives as radical precursors in ATRA processes. Also, the phosphonate derivative **23** proved to be reactive (47 % yield). Interestingly, the reaction with CF_2Br_2

as radical precursor gave straightforward access to the synthetically versatile BCA products **24** and **25**, in 85 % and 55 % yield, respectively. To our delight, other highly diverse radical precursors, including benzyl derivatives, ketones, esters, Weinreb amide, and alkynes were all found to be competent substrates, affording products **26–32** in high yields (up to 87 %).The reaction took place also with the substrates for which π–π interactions were minimal or not possible. In these examples, we assume that a classical SET manifold occurs for the generation of the key RCF_2 radical and final CF_2–BCA product formation. Finally, we proved the robustness of the method with more complex biologically relevant substrates. We efficiently installed the CF_2–BCA hybrid bioisostere into paracetamol, tyramine, and D-galactose derivatives, giving access to the products **33–35** in up to 76 % yield. Also, aminoacids and short peptides: L-tryptophan, L-phenylalanine, and the Gly-Ala derivatives delivered the corresponding hybrid bioisosteres **36–39** in good to high yields (up to 75 %). Of note, the reactions proceeded well also when in presence of free phenolic OH, or amidic and indolic NH groups, proving the robustness and high selectivity of the developed method.

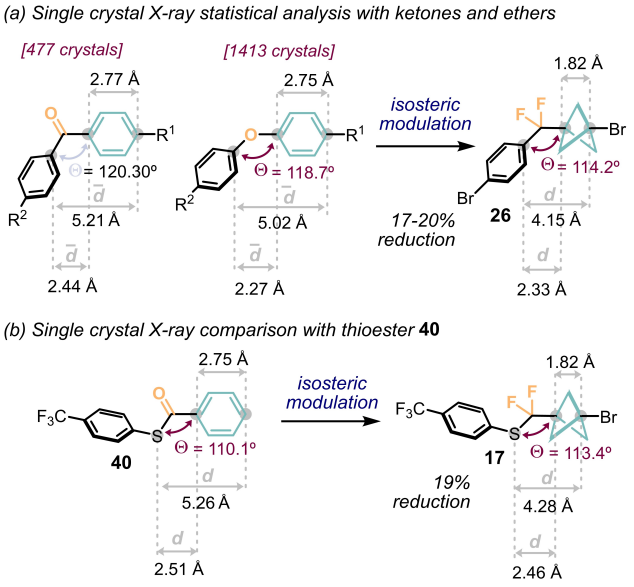

Figure 3. Structural changes associated with the substitution of a) an aryl ketone, aryl ether or b) aryl thioester moieties with the corresponding hybrid CF_2-BCP bioisostere. Structures determined by single-crystal X-ray diffraction.

Solid state analysis

By slow solvent evaporation, we managed to grow the crystals of the products **17**, **26**, **35** and **39** (See Supporting Information, Section E). Single crystal X-ray diffraction (SC-XRD) of these new type of CF_2-BCPs allowed us to perform comparative studies in the solid state, evaluating the structural changes associated with the replacement of an aryl ketone (ArCO) or an aryl ether (ArO) unit with the CF_2–BCP bioisostere.[16]

We thus compare the distances of the distal atoms of the –ArCO–, –ArO– and –CF_2BCP– units in a series of X-ray data (Figure 3a). In 477 molecular structures containing the ArCO unit, the average distance ($\bar{d}$) found was to be 5.21 Å, whereas in the case of aryl ethers (ArO), the $\bar{d}$ was found to be 5.02 Å considering the data of 1413 crystals bearing this unit.[17] The X-ray analysis of the crystal of compound **26** showed that the change for the CF_2-BCP bioisostere results in a 17–20 % reduction of the distance between terminal atoms.

Consistently, a 19 % reduction in distance was observed in the crystals of the thioester **40** and the CF_2–BCP derivative **17** (Figure 3b). Under both analyses, the reduction of the distance is mainly attributed to the shorter transannular distance between the C1 and C3 atoms of the single BCP unit [$d_{C1\text{-}C4}$ (Ar) = 2.77–2.75 Å vs. $d_{C1\text{-}C3}$ (BCP) = 1.82 Å]. On the other hand, the replacement of the C=O or O fragment for the CF_2 unit corresponds to minimal distance variations (1–5 %). Al together these observations indicate that the main structural variations of the –ArCO– or –ArO–⟶CF_2–BCP hybrid bioisostere are in line with the well-established Ph→BCP isosteric replacement.

Products Derivatisations

To demonstrate the synthetic versatility of the CF_2–BCA products, we performed various products manipulations (Figure 4). First, the sulfonyl moiety of product **10** was removed upon reductive cleavage with Mg in MeOH-d_4, giving access to the valuable $^2HCF_2$–BCP product **41** (Figure 4a). It is anticipated that these deuteration routes are particularly relevant for tagging purposes.[18] Next, product **31**, bearing an alkyne unit, proved to be a suitable intermediate for both Cu-catalyzed click reaction[19] and Sonogashira coupling,[20] affording the products **43** and **45** in 70 % and 59 % yield, respectively (Figure 4b). Lithiation of product **14** followed by reaction with different electrophiles, including 4-fluorobenzaldehyde (**47**) or CO_2, gave access to the products **48** and **49** bearing an alcohol, or a carboxylic acid, respectively (Figure 4c).[21] Interestingly, the CF_2–BCP-organolithium intermediate **46** also engaged in a Negishi coupling with 2-bromopyiridine (**50**), affording the product **51** in 24 % yield. Finally, the reaction of **46** with MeOH-d_4 allowed the straightforward installation of deuterium (^2H) in the BCP unit, forming product **52** in 66 % yield.[22]

Synthesis of LTA_4 Hydrolase, Inhibitor Analogue and Molecular Docking Studies

Aiming at evaluating the replacement of an aryl ether moiety with the CF_2–BCA hybrid bioisostere in a bioactive molecule, we selected the LTA_4 hydrolase inhibitor **1** and targeted the corresponding analogue **53** (Figure 5a). Interestingly, we found that **53** shows enhanced lipophilicity and water solubility as indicated by the computed cLogP and

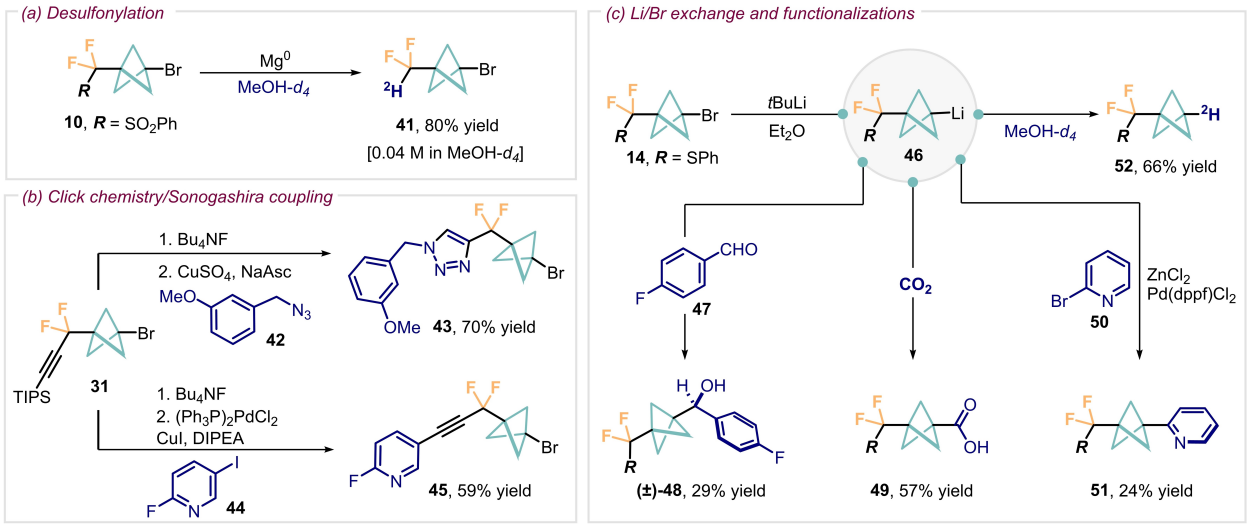

Figure 4. Product derivatisations with diverse CF_2-BCA products **7**.

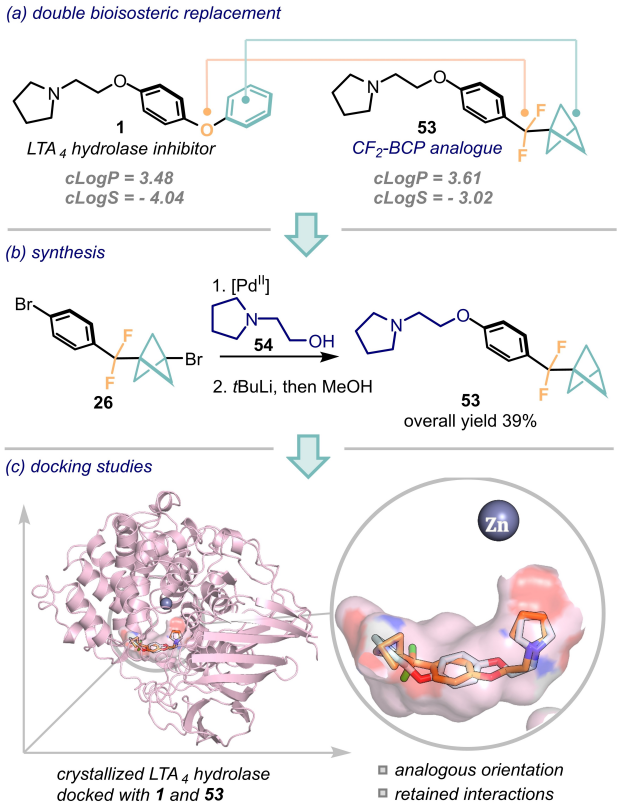

Figure 5. a) Selected LTA_4 hydrolase inhibitor **1** and targeted CF_2-BCP analogue **53**. b) Synthesis of **53**. [Pd^{II}] = AdCyBrettPhos Pd G3. c) Calculated structure of **1** (light blue backbone) and **53** (orange backbone) within the hydrophobic pocket of the zinc metalloenzyme LTA_4 hydrolase (pink backbone). Best docking poses for **1** and **53** are shown.

cLogS values. With these promising indications, we next performed the synthesis of **53**. We were able to readily convert compound **26** into **53**, through a two-steps process involving: i) a C–O cross-coupling reaction with the amino-alcohol **54**,[22] and ii) a Li/Br exchange followed by protonation, with an overall yield of 39 % (Figure 5b).

Having **53** in hand, we interrogated docking studies on the spatial organization of this molecule within the LTA_4 hydrolase (Figure 5c).[23] Interestingly, both compounds were found to bind to the protein with analogous orientation within an L-shaped hydrophobic cavity in proximity of the Zn-binding site. This binding mode is in good agreement with those observed for related small molecules co-crystallized with the LTA_4 hydrolase enzyme.[24] More in detail, the inhibitor **1** showed polar interactions between the pyrrolidine moiety and the protein backbone (Gln136 and Ala137) and a π–π stacking between the *p*-disubstituted aryl ring and the lateral chain of Phe314, while placing the phenoxy ring at the end of the hydrophobic cavity (see Figure S23 in the Supporting Information). Importantly, these key interactions are fully preserved for the analogue **53**, whose BCP moiety, as for the phenoxy ring of **1**, is placed at the end of the hydrophobic cavity. Hence, the overall bioisosteric replacement of the phenoxy ring for the CF_2–BCP unit does not significantly alter the binding mode within the LTA_4 hydrolase. These promising data open the way to the following in vitro biological evaluations of such molecule, as well as other CF_2–BCA derivatives as effective bioisosteric replacements.

Conclusion

In summary, we have developed a general and mild photochemical strategy to the synthesis of CF_2–BCA hybrid bioisosteres. The process is catalyzed by the acridine **PC3**, that upon light-excitation, promotes the generation of the key R–CF_2 radical, either by direct reduction of the starting substrate or via an EDA-complex manifold. Then, the R–CF_2 radical reacts with the propellane through an ATRA process. The generality of the method was proven for structurally diverse substrates including amines, amides,

esters, aminoacids or carbohydrates. Structural analysis on the single crystal of products **17**, **26**, **35** and **39** revealed a structural contraction of the corresponding aromatic ketone or aromatic ether of 17–20 %, thus profiling the possible utilization of the CF_2–BCA core as a hybrid bioisostere for such scaffolds. These findings were corroborated by docking studies, which revealed that the binding mode of a known LTA_4 hydrolase inhibitor **1** was retained in the CF_2-BCP analogue **53**. We foresee the utilization of the developed synthetic platform to access new fluorinated hybrid bioisosteres, while opening the way to their widespread use in medicinal chemistry settings.

Acknowledgements

This work was supported by MUR (Ministero dell'Università) PRIN 2020927WY3_002, and (European Research Council) ERC-Starting Grant 2021 SYNPHOCAT 101040025 (L.D.). P.C. thanks the University of Padova and the European Union—NextGenerationEU for financial support via the grant program STARS@UNIPD, Frame-PSII. G.G. thanks the University of Padova for a MSCA Seal of Excellence @Unipd PhotoFix-Zyme fellowship and MUR for a Young Researchers, Seal of Excellence fellowship. Dr. Davide Bassani (University of Padova),Dr. Santiago Cañellas (Janssen, Toledo), and Dr. Elena Lenci (University of Florence) are acknowledged for insightful discussions. Simone Baldon (University of Padova) is acknowledged for the experimental support during the product manipulations. Chiesi Farmaceutici SpA and Dr Davide Balestri are acknowledged for the support with the D8 Venture X-ray equipment.

Conflict of Interest

The authors declare no conflict of interest.

Data Availability Statement

The data that support the findings of this study are openly available in chemrxiv at https://chemrxiv.org/engage/chemrxiv/article-details/640f2176e53eff1af31073a2.

Keywords: Fluorine Chemistry · Hybrid Bioisostere · Photoredox Catalysis · Propellanes · Sustainable Synthesis

[1] a) N. A. Meanwell, *J. Med. Chem.* **2011**, *54*, 2529–2591; b) N. A. Meanwell, *Chem. Res. Toxicol.* **2016**, *29*, 564–616; c) N. A. Meanwell, *J. Med. Chem.* **2018**, *61*, 5822–5880; d) E. G. Tse, S. D. Houston, C. M. Williams, G. P. Savage, L. M. Rendina, I. Hallyburton, M. Anderson, R. Sharma, G. S. Walker, R. S. Obach, M. H. Todd, *J. Med. Chem.* **2020**, *63*, 11585–11601.

[2] T. D. Penning, N. S. Chandrakumar, B. B. Chen, H. Y. Chen, B. N. Desai, S. W. Djuric, S. H. Docter, A. F. Gasiecki, R. A. Haack, J. M. Miyashiro, *J. Med. Chem.* **2000**, *43*, 721–735.

[3] P. K. Mykhailiuk, *Org. Biomol. Chem.* **2019**, *17*, 2839–2849.

[4] Y. L. Goh, Y. T. Cui, V. Pendharkar, V. A. Adsool, *ACS Med. Chem. Lett.* **2017**, *8*, 516–520.

[5] a) S. Meyer, J. Häfliger, R. Gilmour, *Chem. Sci.* **2021**, *12*, 10686–10695; b) Y. Kraemer, C. Ghiazza, A. N. Ragan, S. Ni, S. Lutz, E. K. Neumann, J. C. Fettinger, N. Nöthling, R. Goddard, J. Cornella, C. R. Pitts, *Angew. Chem. Int. Ed.* **2022**, *61*, e202211892.

[6] D. C. Blakemore, L. Castro, I. Churcher, D. C. Rees, A. W. Thomas, D. M. Wilson, A. Wood, *Nat. Chem.* **2018**, *10*, 383–394.

[7] a) N. Erdeljac, K. Bussmann, A. Schöler, F. K. Hansen, R. Gilmour, *ACS Med. Chem. Lett.* **2019**, *10*, 1336–1340; b) N. Erdeljac, C. Thiehoff, R. P. Jumde, C. G. Daniliuc, S. Höppner, A. Faust, A. K. Hirsch, R. Gilmour, *J. Med. Chem.* **2020**, *63*, 6225–6237.

[8] a) G. E. M. Crisenza, D. Mazzarella, P. Melchiorre, *J. Am. Chem. Soc.* **2020**, *142*, 5461–5476; b) C. G. S. Lima, T. de M Lima, M. Duarte, I. D. Jurberg, M. W. Paixão, *ACS Catal.* **2016**, *6*, 1389–1407.

[9] A. Rentería-Gómez, W. Lee, S. Yin, M. Davis, A. R. Gogoi, O. Gutierrez, *ACS Catal.* **2022**, *12*, 11547–11556.

[10] J. B. Sap, C. F. Meyer, N. J. Straathof, N. Iwumene, C. W. Am Ende, A. A. Trabanco, V. Gouverneur, *Chem. Soc. Rev.* **2021**, *50*, 8214–8247.

[11] S. Wang, G. Force, J.-F. Carpentier, Y. Sarazin, C. Bour, V. Gandon, D. Lebœuf, *Org. Lett.* **2021**, *23*, 2565–2570.

[12] a) J. Mateos, F. Rigodanza, A. Vega-Peñaloza, A. Sartorel, M. Natali, T. Bortolato, G. Pelosi, X. Companyó, M. Bonchio, L. Dell'Amico, *Angew. Chem. Int. Ed.* **2020**, *59*, 1302–1312; b) C. Rosso, S. Cuadros, G. Barison, P. Costa, M. Kurbasic, M. Bonchio, M. Prato, L. Dell'Amico, G. Filippini, *ACS Catal.* **2022**, *12*, 4290–4295; c) T. Bortolato, G. Simionato, M. Vayer, C. Rosso, L. Paoloni, E. M. Benetti, A. Sartorel, D. Lebœuf, L. Dell'Amico, *J. Am. Chem. Soc.* **2023**, *145*, 1835–1846; d) S. Cuadros, C. Rosso, G. Barison, P. Costa, M. Bonchio, M. Prato, G. Filippini, G. L. Dell'Amico, *Org. Lett.* **2022**, *24*, 2961–2966.

[13] J. Nugent, C. Arroniz, B. R. Shire, A. J. Sterling, H. D. Pickford, M. L. Wong, S. J. Mansfield, D. F. Caputo, B. Owen, J. J. Mousseau, F. Duarte, E. A. Anderson, *ACS Catal.* **2019**, *9*, 9568–9574.

[14] a) T. Kawasaki, N. Ishida, M. Murakami, *J. Am. Chem. Soc.* **2020**, *142*, 3366–3370; b) Z. Wang, X. Ji, T. Han, G. J. Deng, H. Huang, *Adv. Synth. Catal.* **2019**, *361*, 5643–5647;c) H. G. Roth, N. A. Romero, D. A. Nicewicz, *Synlett* **2016**, *27, 714–723*.

[15] a) E. JináCho, *Chem. Commun.* **2014**, *50*, 12884–12887; b) J. D. Nguyen, J. W. Tucker, M. D. Konieczynska, C. R. Stephenson, *J. Am. Chem. Soc.* **2011**, *133*, 4160–4163; c) J. W. Tucker, Y. Zhang, T. F. Jamison, C. R. Stephenson, *Angew. Chem. Int. Ed.* **2012**, *51*, 4144–4147; d) A. Granados, R. K. Dhungana, M. Sharique, J. Majhi, G. A. Molander, *Org. Lett.* **2022**, *24*, 4750–4755.

[16] Deposition Numbers 2226178 (for **17**), 2217587 (for **26**), 2226179 (for **35**), and 2217588 (for **39**) contain the supplementary crystallographic data for this paper. These data are provided free of charge by the joint Cambridge Crystallographic Data Centre and Fachinformationszentrum Karlsruhe Access Structures service.

[17] Data available in the CCDC database: https://www.ccdc.cam.ac.uk/.

[18] a) S. Kopf, F. Bourriquen, W. Li, H. Neumann, K. Junge, M. Beller, *Chem. Rev.* **2022**, *122*, 6634–6718; b) J. Atzrodt, V. Derdau, W. J. Kerr, M. Reid, *Angew. Chem. Int. Ed.* **2018**, *57*, 1758–1784.

[19] J. E. Moses, A. D. Moorhouse, *Chem. Soc. Rev.* **2007**, *36*, 1249–1262.

[20] R. Chinchilla, C. Nájera, *Chem. Rev.* **2007**, *107*, 874–922.
[21] D. F. Caputo, C. Arroniz, A. B. Dürr, J. J. Mousseau, A. F. Stepan, S. J. Mansfield, E. A. Anderson, *Chem. Sci.* **2018**, *9*, 5295–5300.
[22] H. Zhang, P. Ruiz-Castillo, S. L. Buchwald, *Org. Lett.* **2018**, *20*, 1580–1583.
[23] A. Stsiapanava, U. Olsson, M. Wan, T. Kleinschmidt, D. Rutishauser, R. A. Zubarev, B. Samuelsson, A. Rinaldo-Matthis, J. Z. Haeggström, *Proc. Natl. Acad. Sci. USA* **2014**, *111*, 4227–4232.
[24] D. R. Davies, B. Mamat, O. T. Magnusson, J. Christensen, M. H. Haraldsson, R. Mishra, B. Pease, E. Hansen, J. Singh, D. Zembower, *J. Med. Chem.* **2009**, *52*, 4694–4715.

Manuscript received: March 14, 2023
Accepted manuscript online: June 1, 2023
Version of record online: June 23, 2023